The influence of systematic structure alterations on the photophysical properties and conjugation characteristics of asymmetric cyanine 5 dyes

S.J. Spa,[a, b] A.W. Hensbergen,[a] S. van der Wal,[a] J. Kuil,[c] F.W.B. van Leeuwen[a, b]

[a] Interventional Molecular Imaging Laboratory, Department of Radiology, Leiden University Medical Center, The Netherlands.

[b] Laboratory of BioNanoTechnology, Wageningen, The Netherlands.

[c] Department of Clinical Pharmacy and Toxicology, Leiden University Medical Center, The Netherlands

[*]Corresponding Author. Albinusdreef 2, 2333 ZA Leiden, The Netherlands *Email:* F.W.B.van_Leeuwenlumc.nl (F.W.B. van Leeuwen)

Keywords: Cyanine dyes, Protein conjugation, Far-red fluorescence, Fluorescence-guided surgery, Molecular imaging

Abstract

The light spectrum above 650 nm allows for good tissue penetration depths, far-red and near-infrared fluorescent dyes are therefore popular fluorophores applied in (bio)medical diagnostics, including image-guided surgery. However, near-infrared fluorescent dyes often suffer from instability and limited brightness, two important features that, together with the labelling efficiency (*e.g.*, non- one- or di-conjugated products) and serum-dye interactions are key elements that drive *in vivo* characteristics. Due to the fact that stability and brightness of far-red fluorophores are often superior over near-infrared dyes, interest in the use of dyes such as Cy5 is increasing. As there are clear indications that the influence of the chemical structure on the (photo)physical properties of a dye is dye-structure-dependent, the (photo)physical properties of ten structural variants of asymmetrical Cy5-(R_1)R_2-(R_3)COOH (R representing the varied substituents) were extensively studied, While stacking in solution was not induced in most of the Cy5 far-red fluorophores, multimers and

stacking characteristics were observed in protein conjugates. And although all dye variants were shown to be stable towards photobleaching, clear differences in brightness and serum interactions were found. Combined, these findings indicate that the chemical substituents prominently influence the photophysical properties of Cy5 dyes, a feature that should be considered when using fluorescent dyes in future tracer development.

1. Introduction

Fluorescent dye-based guidance during surgical interventions is being recognised as an improvement in the accuracy of clinical care [1–3]. In clinical trials, fluorescence imaging has been used as a sole modality or in a bimodal/hybrid form, wherein it extends the field of nuclear medicine [4]. While fluorescence emissions across the light spectrum have been used for image guided surgery [2], emphasis lies on the use of dyes emitting in the far-red (650 nm < λ_{em}< 750 nm) or near-infrared (NIR) region ($\lambda_{em} \geq$ 750 nm)[5]. This theoretical preference can be attributed to the enhanced penetration depths and limited auto-fluorescence in at these wavelengths.

Unfortunately, the dye chemistry, stability and/or photophysical properties of near-infrared dyes are limited compared to dyes emitting at lower wavelengths. For example, the most commonly applied near-infrared dye indocyanine green (**ICG**) is prone to stack/aggregate from aqueous solutions and has a low quantum yield (Q_F = 0.3% in H_2O)[6]. More experimental dyes such as IRdye 800CW also have a low quantum yield (Q_F = 3.4% in H_2O)[7] and have been shown to be chemically unstable with respect to endogenous nucleophiles [8]. These limitations have boosted the interest in far-red dyes. For instance, methylene blue (**MB**), a clinically applied dye with a weak far-red fluorescence emission (Q_F = 3% in H_2O) has been applied in humans to image ureters [9], parathyroid glands [10], and bile ducts [11], despite the FDA warning against its use [12]. As an alternative, the Cy5 family provides relatively bright (~ $3 \cdot 10^4$ $M^{-1} \cdot cm^{-1}$, $Q_F \approx$ 20 % in H_2O)[13] far-red fluorophores and encompasses many structural variations. A prime example of a Cy5-based imaging agent in clinical use is found in GE-137 (now EM-137), a Cyanine 5 (Cy5)-labelled c-Met-targeting peptide that was

effectively used for identification of colorectal polyps in humans [14]. Furtermore, the Cy5-containing nanoparticles ^{124}I- cRGDY-PEG-C have been used to target metastatic melanoma [15].

To convert Cy5-dyes into imaging agents of value for fluorescence-guided surgery, these dyes have to be conjugated to targeting vectors. When a targeting vector has multiple conjugation sites, *e.g.* a protein, labelling may not be straightforward. A ratio of one dye per targeting vector is generally aimed at, but the final product often consists of, *e.g.*, a mixture of none-, one-, di-, and/or tri-dye conjugated imaging agents. In case multiple dyes are located on a single targeting vector, the occurrence of dye-stacking or Förster Resonance Energy Transfer (FRET) between the dyes can cause luminescence quenching, a feature that reduces the brightness of the imaging agent [8].

Conjugation of imaging labels, and especially an excess thereof, may also negatively influence the binding specificity and pharmacokinetics of a targeting vector. Dependent on the size of the targeting vector, the scale of these effects varies [16], being most prominent when relatively small peptides are used [14,17]. Nevertheless, this effect is also reported for larger proteins, *e.g.*, mAb conjugates [18]. When dyes express an affinity for serum proteins such as human serum albumin, *e.g.*, **ICG** and Cy5-(Ar)SO_3-(Ar)SO_3 [19–21], this may further effect the tracer pharmacokinetics.

In order to determine the influence of the structure of a florescent dye on its utility as an imaging label, ten Cy5 analogues were synthesised and compared with the reference compound **MB**. By alternating the aromatic (R_1 and R_3) and alkyl substituents (R_2), molecular variations on Cy5-(R_1)R_2-(R_3)COOH were systematically evaluated for their photophysical properties, chemical- and photo-stability, serum protein interaction, dye–dye stacking tendencies, and conjugation efficiency (Figure 1).

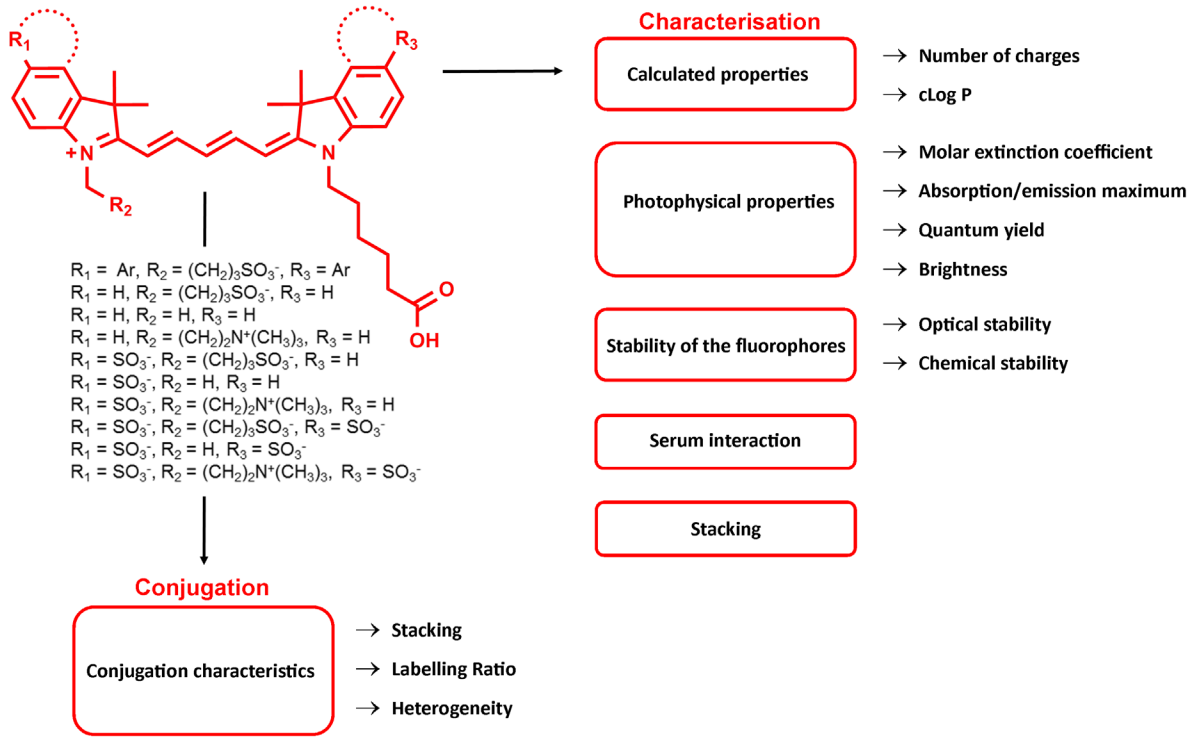

Figure 1. Overview of the subjects and fluorophore properties investigated and discussed throughout the article.

2. Experimental

2.1. Materials and reagents

For the synthesis of the fluorophores (Compound **1-21**), cLog P calculations, and information on the materials used, please refer to the Supporting information (SI). The electron density modelling is reported in Ref [22]

2.2 Ubiquitin Labelling (compound 22–30)

Stock solutions of the NHS-activated fluorophores (**12–21,** see SI) were prepared in DMSO and the percentage of activated dye was determined by HPLC (see also SI 'NHS activation'). Subsequently, Ubiquitin (16 nmol) was dissolved in 500 µL of phosphate buffer (0.1 M, pH 8.4, 2.67 g HNa_2PO_4 + 0.14 g H_2NaPO_4 in 200 µL H_2O). Appropriate amounts of the fluorophore stock solution were added, ensuring that each sample contained 3 equivalents activated dye (50 nmol, 100 µM final

concentration) and that the DMSO content in the final solution was < 10%. The mixtures were shaken at room temperature for 6.5 h and the labelled Ubiquitin was washed with PBS by filtration over a 3K Amicon® filter subsequently. When the filtrate was no longer blue, the residue was collected in 100 µL PBS.

Dye–Ubiquitin conjugates were analysed by mass spectrometry and absorption measurements using a NanoDrop. To determine the average labelling ratio, the dye concentration was calculated from absorption measurements in DMSO around 650 nm (Table 1) and the obtained values were then divided by the known protein concentration (0.16 mM). For compound **30** significant precipitation was observed after the reaction, therefore the protein content in this sample also was determined by absorption (ε_{280} = 1490 $M^{-1}\cdot cm^{-1}$, calculated from the amino acid sequence) [23]. Since Cy5 also shows absorbance at this wavelength, a correction was made by measuring the absorbance of free dye at this concentration and subtracting it from the absorbance value measure for the dye containing Ubiquitin.

2.3 Photophysical properties

2.3.1. Molar extinction coefficient (ε) *of compound **1**–**11***

To obtain a 4 mM stock solution of **MB** (**1**), 3.2 mg Methylene blue hydrate (Fisher Scientific) was dissolved in 4 mM ethylene carbonate in DMSO-d_6 (1500 µL) and the exact concentration was determined by NMR using ethylene carbonate as internal standard [8].

To allow for absorption measurements, the 4 mM stock solutions of the dyes in DMSO-d_6 (**1**-**11**, for details, see SI) were diluted to 100 µM in DMSO, H_2O or PBS. From the 100 µM concentration, 50 µM and 5 µM concentrations were made from which further two-fold dilution in the same medium followed to obtain a final concentration range of 100, 50, 25, 12.5, 5, 2.5, 1.2, 0.6, and 0.3 µM, respectively. Absorption spectra were measured using 1 mL disposable plastic cuvettes (l = 1 cm; Brand, Germany) for concentrations ≤ 5 µM, quartz cuvettes (l = 0.1 cm; Hellma standard cell, Macro) for 12, 25, and 50 µM concentrations, and two glass microscopy slides held together with a

0.14 mm thick PET plastic spacer for the 100 µM concentration to keep the signal below 1.5 AU. Optical density was measured 10 minutes after preparation and the plotted absorbance was normalised for cuvette path length and concentration. The ε was then determined by applying a linear regression coefficient.

*2.3.2. Absorbance spectra of the labelled Ubiquitin (**22**–**30**)*

The Ubiquitin solutions collected after synthesis (for synthesis procedures see SI) were diluted 100 x in PBS and the absorbance spectra were measured using NanoDrop. Subsequently, the obtained spectra were normalised for dye concentration.

*2.3.3. Quantum yield and emission maximum determination of compound **1**–**11** and **22**–**30***

Fluorescence spectra were measured at λ_{ex} = 606 nm for compounds **3**–**11** and the Ubiquitin conjugates **22**–**30**, and λ_{ex} = 620 nm for **1**–**2**, using 1 cm disposable plastic 4.5 mL cuvettes (Kartell, Germany). 3 mL of 0.5 µM dye was prepared in PBS (**1**–**11**, **22**–**30**) by first preparing 100 µM solutions in PBS from the DMSO-d_6 dye stock (**1**–**9** and **MB** solutions) or from dilutions of the Ubiquitin conjugates (**22**–**30**) (see SI for synthesis). To determine the quantum yield, the absorbance at λ = 606 (compounds **3**–**11** and **22**–**30**) or λ = 620 nm (compound **1**–**2**) of 0.5 µM and 0.25 µM were measured and correlated with the integrated fluorescent emission. The regression coefficient of the resulting plot for the unknown dyes was then compared to the regression coefficient of Cy5-(SO_3)COOH-(SO_3)COOH (Figure 2), which has a known quantum yield (Q_F = 27%) [13].

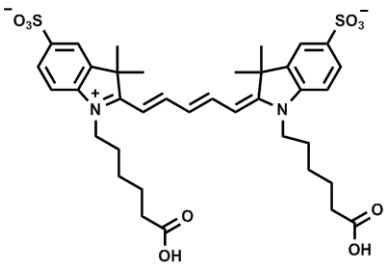

Figure 2. Chemical structure of the reference compound applied for the quantum yield determination; Cy5-(SO_3)COOH-(SO_3)COOH.

2.4 Stability

*2.4.1 Chemical stability of compound **1**–**11** towards glutathione*

Solutions of 0.25 mM dye (from DMSO-d_6 NMR solutions) and 0.5 mM glutathione in 4-(2-hydroxyethyl)-1-piperazine-ethanesulfonic acid buffer (HEPES, 0.1 M, pH 7.4) were freshly made. Prior to the addition of glutathione to the HEPES buffer, nitrogen was bubbled through the HEPES buffer to remove oxygen and reduce the rate of disulfide formation of glutathione. The solutions were immediately put into the sample manager (37 °C) of a Waters Acquity UPLC-MS system equipped with an Acquity UPLC photodiode array detector, an SQ Detector mass spectrometer and a Waters BEH C18 130 Å 1.7 µm (100 × 2.1 mm) column (flow rate: 0.5 mL/min). Analysis was performed every 30 minutes using a gradient of 0.05% TFA in H_2O/0.04% TFA in CH_3CN 95:5 to 0.05% TFA in H_2O/0.04% TFA in CH_3CN 5:95 in 5.44 minutes. The stability of the dyes was calculated relative to the integration of the chromatogram at t = 0 h.

*2.4.2 Optical stability of compound **1**–**11***

For the optical stability measurements, a prototype Karl Storz camera setup (KARL STORZ Endoskope GmbH & Co. KG, Tuttlingen, Germany) was applied. This camera setup included an IMAGE1 S H3-Z FI Three-Chip FULL HD camera head equipped with a 0^o laparoscope in combination with an IMAGE 1 S CONNECT module, an IMAGE 1 S H3-LINK link module and a Cy5-modified D-light C light source (590-680 nm emission). A standard eyepiece adaptor containing a filter that passes through light between 640–720 nm (Cat no. 20100034; KARL STORZ Endoskope GmbH & Co. KG) was placed between the camera and the laparoscope to image the Cy5 fluorescence.

From the DMSO-d_6 dye stock solutions (see synthesis in SI) 100 µM solutions in PBS were prepared. Subsequently, from the 100 µM solutions, 3.0 mL of 1 µM solutions were prepared in 4.5

mL disposable cuvettes (Kartell, Germany). The cuvettes were placed in front of the prototype Karl Storz camera and illuminated at maximum intensity for 30 minutes. At 5-minute intervals the fluorescence was measured with λ_{ex} = 602 nm. The reduction in fluorescence intensity was plotted and normalised relative to the fluorescence intensity obtained at t = 0 minutes.

2.5 Serum protein interaction

Serum protein binding was assayed using the single-use Rapid Equilibrium Dialysis (RED) plate kit with an 8 kD MWCO (Pierce, Thermo Scientific). Serum (300 µL, fetal bovine serum, heat inactivated) was placed into the dialysis chamber and phosphate buffer (500 µL, 100 mM phosphate and 150 mM NaCl, pH = 7.2) was placed into the reservoir chamber. The dyes were added from a DMSO stock (100 µM, 3 µL) to the dialysis chamber (n = 2) and in duplicate samples (n = 2) to the reservoir chamber. The plate was subsequently closed using sealing tape and incubated at room temperature on a rocking shaker for 18 h, after which 100 µL aliquots were withdrawn from both chambers for each dye. 100 µL phosphate buffer was then added to the aliquots containing serum, and 100 µL serum was added to the aliquots containing phosphate buffer. All aliquots were transferred to a white 96 well plate (Greiner Lumitrac 600) and fluorescence was quantified at λ_{ex} = 620 nm using a PerkinElmer LS 55 fluorometer (equipped with a red-sensitive detector and a plate-reader attachment). Serum protein binding percentages were calculated using the manufacturer's protocol (eq. 1):

$$\%_{bound} = \left(100 - \frac{[buffer\ chamber]}{[serum\ chamber]}\right) \cdot 100 \qquad \text{eq. 1}$$

2.6 Stacking behaviour of compound 1–11 in different solvents

To determine the stacking behaviour of the dyes (**1**–**11**) in DMSO, H_2O or PBS, the same dilutions and absorbance measurements were performed as described for measuring the molar extinction coefficient (chapter 2.3.1). For a more detailed description please refer to Ref [22].

3. Results and Discussion

3.1 Chemical properties

The number of charges, and calculated Log P (cLog P) values of the investigated fluorophores are given in Figure 3. Overall, the calculated net charge decreased with increasing number of sulfonate moieties on the aromatic ring, which also resulted in decreasing cLog P values. The highest cLog P value was, as expected, calculated for compound **2** due to the presence of additional benzene rings. The lowest cLog P value was found for compound **11,** as a result of the high total number of charges (5). The cLog P value of **MB** (**1**) was most similar to the cLog P value calculated for compound **6**.

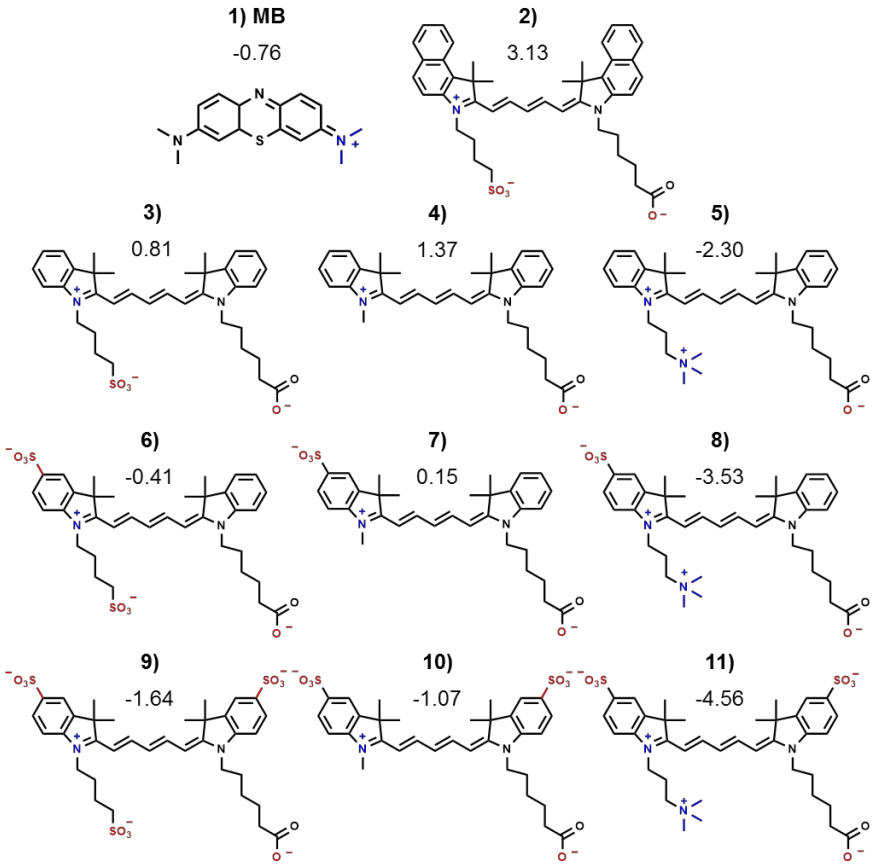

Figure 3. The cLog P values of the compounds **1**–**11**. In the compound structures the positively charged groups are indicated in blue and negatively charged groups are indicated in red.

3.2 Photophysical properties

The molar extinction coefficient (ε) was calculated *via* the regression coefficient between the concentration and the absorbance determined from a linear concentration range between 0.3–5 μM in DMSO, H_2O, and PBS. In DMSO, except for compounds **2**, **4** (ε ≈ 185.000 $M^{-1}cm^{-1}$) and **MB** (**1**, ε = 84.000 $M^{-1}cm^{-1}$), all dyes had ε > 200.000 $M^{-1}cm^{-1}$. The ε determined for **MB** in DMSO was in line with the literature, which reports values between 70.000 and 95.000 $M^{-1}cm^{-1}$ [24,25]. For compounds **3**–**8** the ε decreased with about 25% when changing the solvent from DMSO to H_2O or PBS. A more substantial decrease (37%) was observed for the more lipophilic compound **2**. Remarkably, for the more soluble compounds with two aromatic sulfonates (**9**–**11**) the change in solvent resulted in a 10% increase in the ε and gave extinction coefficients of 242.000, 220.000 and 231.000 $M^{-1}cm^{-1}$ in PBS respectively (Table 1).

The absorption/emission maxima of the Cy5 fluorophores (**2**–**11**) observed in DMSO had Stokes shifts of about 20 nm (Table 1) while **MB** (**1**) had a Stokes shift of 16 nm. Changing the solvent from DMSO towards H_2O or PBS caused a hypsochromic shift in the absorption/emission maximum of 10 nm for **2**–**11** and only a minor shift (5 nm) for **MB**. Comparison of the absorption/emission maxima (Table 1) with the structure of the dyes (Figure 3), revealed that all compounds with a sulfonate on both aromatic rings (**9–11**) displayed a slight bathochromic shift of around 5 nm in their maxima. This bathochromic shift has also been reported for other Cy5-fluorophores [26]. This effect was, however, not observed when no or just one aromatic sulfonate was present at this location (*e.g.*, **9** vs **3** and **6**, Table 1).

In practice, the environment of the fluorophores will be aqueous, hence the quantum yields measurements were performed in PBS and related to that of Cy5-(SO_3)COOH-(SO_3)COOH (Φ_F = 27%) [13]. In line with the above-presented molar extinction coefficients, the quantum yields of compounds **9**, **10**, and **11** were also the highest (23%) from the series; the other Cy5-dye derivatives displayed quantum yields around 13% or lower (Table 1). In contrast, **MB** yielded a quantum yield of merely 3%. It is interesting to note that the quantum yields did not alter significantly upon changing the alkyl substituent (*e.g.*, **3** vs **4** vs **5,** Table 1), or changing the number of aromatic sulfonates from

0 to 1 (*e.g.*, **3** vs **6**). As Fisher *et al.* suggested [27], a clear trend between the structure of dyes and the quantum yield seems to be missing.

Table 1. Photophysical properties of compound **1–11,** including the quantum yields of **22–30**.

Dye	ε in DMSO [a] ($M^{-1}\cdot cm^{-1}$)	ε in water [a] ($M^{-1}\cdot cm^{-1}$)	ε in PBS [a] ($M^{-1}\cdot cm^{-1}$)	$\lambda_{ex}/\lambda_{em}$ in DMSO (Stokes shift; nm)	$\lambda_{ex}/\lambda_{em}$ in H_2O and PBS (Stokes shift; nm)	Φ_F in PBS [b] Non-conjugated	Φ_F in PBS [b] Conjugated (**22–30**)
MB (1)	$84 \cdot 10^3$	$77 \cdot 10^3$	$71 \cdot 10^3$	670/686 (16)	665/679 (14)	3%	n.a. [c]
2	$181 \cdot 10^3$	$113 \cdot 10^3$	$112 \cdot 10^3$	688/710 (22)	678/695 (17)	10%	n.a. [c]
3	$200 \cdot 10^3$	$199 \cdot 10^3$	$203 \cdot 10^3$	655/671 (16)	643/659 (16)	14%	5%
4	$188 \cdot 10^3$	$176 \cdot 10^3$	$174 \cdot 10^3$	647/667 (20)	640/656 (16)	13%	10%
5	$218 \cdot 10^3$	$193 \cdot 10^3$	$193 \cdot 10^3$	658/677 (19)	638/658 (20)	13%	12%
6	$228 \cdot 10^3$	$206 \cdot 10^3$	$206 \cdot 10^3$	655/675 (20)	643/660 (17)	13%	9%
7	$238 \cdot 10^3$	$176 \cdot 10^3$	$212 \cdot 10^3$	653/672 (19)	642/658 (16)	13%	3%
8	$200 \cdot 10^3$	$146 \cdot 10^3$	$149 \cdot 10^3$	647/673 (26)	637/657 (20)	9%	14%
9	$219 \cdot 10^3$	$245 \cdot 10^3$	$242 \cdot 10^3$	660/679 (19)	648/664 (16)	22%	21%
10	$204 \cdot 10^3$	$233 \cdot 10^3$	$220 \cdot 10^3$	658/677 (19)	646/662 (16)	23%	14%
11	$209.0 \cdot 10^3$	$223 \cdot 10^3$	$231 \cdot 10^3$	659/677 (18)	645/661 (16)	23%	20%

a) Fresh dilutions from the DMSO stock were made and measured within 2 hours

b) Relative quantum yield, compared to Cy5-(SO3)COOH-(SO3)COOH (Φ_F = 27%)[13]

c) Labelling was not successful

With ε for molar extinction coefficient, $\lambda_{ex}/\lambda_{em}$ for excitation/emission wavelength, Φ_F for quantum yield and n.a. for not applicable.

Although emphasis is generally placed on the molar extinction coefficient or quantum yield individually, the combination of both properties, *i.e.*, the brightness (quantum yield x molar extinction coefficient)[28], often gives more insight in the optical capability of the fluorophores. This difference also becomes apparent from Figure 4, where all 11 fluorophores are imaged by a prototype Karl Storz camera setup (λ_{ex} = 590–680 nm, data collection between 640–750 nm). For proper *in vivo* visualisation, a signal-to-background ratio (*e.g.*, tumour to muscle) of at least 2 is required [29]. On the basis of the signal-to-background ratio calculated from Figure 4, one can

deduct that a brightness > $1 \cdot 10^4$ $M^{-1} \cdot cm^{-1}$ is required to achieve a signal to background ration > 2. With a brightness of $3 \cdot 10^3$ $M^{-1} \cdot cm^{-1}$ and a signal to background ration of 1.6, **MB** fluorescence was considered too weak to be detected accurately (Figure 4B). Since fluorescence imaging of **MB** has already been used in clinical trials, this finding underlines the medical potential of the relatively bright Cy5 dyes [30].

A

B

Dye	Brightness ($10^3 \cdot M^{-1} \cdot cm^{-1}$)	Signal to background ratio
MB (1)	3	1.6
2	11	2.1
3	28	2.3
4	23	2.9
5	25	2.3
6	27	2.8
7	28	3.0
8	13	2.2
9	53	4.0
10	51	3.9
11	53	3.9

Figure 4. Brightness of the fluorophores in PBS (1 µM) measured by Storz camera (A) or calculated (B). From the image (A) the corresponding signal to background ratios were calculated (B). Overall, the fluorophores with two aromatic sulfonates (**9**–**11**) emit the brightest fluorescence, while **MB** is hardly visible at all (signal to background ratio < 2).

Figure 4 indicates that the fluorophores with two aromatic sulfonates (**9**–**11)** possess the best optical properties. It is known that electron-withdrawing groups, *e.g.*, sulfonates, substituted on the aromatic ring, increase the brightness of such fluorophores [31]. Interestingly, despite their match in brightness, Spartan calculations revealed differences in the theoretical electron densities (Figure 2 in Ref [22], please refer to Ref [22] for further details). Hence, in line with the report by Levitus *et al.*,[32] the positive effect of aromatic sulfonates on the optical properties might not solely

lie in the electrostatic withdrawing capacity. According to the combined data in Table 1 and Figure 2 in Ref [22], the concept of reinforced conformal stability seems to offer a more probable explanation for the sulfonate induced increase in fluorescence brightness; *cis*-*trans* photoisomerisations of the central methine bridge influences the fluorescence brightness [33]. In the ground state, the main conformation of the Cy5 dyes is the *trans*-conformation [32]. However, when excited, the methine bridge can rotate around its C–C bonds, twisting towards the *cis*-conformation [32,34]. In the *cis*-conformation, the most probable route towards the ground state is *via* non-luminescent internal conversion due to the high overlap in the vibronic wave functions (Frank-Condon factor) [26]. It has been speculated that sulfonation of the aromatic rings increases the stability of the *trans*-conformation, thereby reducing the rate of *cis*-*trans* photoisomerisation [32,34] and increasing the fluorescence brightness.

3.3 Stability of the fluorophores

As the fluorophores **2**–**11** were synthesised with a future use in image-guided surgery in mind, their optical stability was tested by exposure to a light source of a dedicated laparoscopic fluorescence camera (λ_{ex} = 590–680 nm). With the exclusion of ambient light, fluorophore solutions of 1 μM in PBS were irradiated for a duration of 30 minutes, with an assessment of their fluorescence intensity at 5-minute intervals. For most compounds, more than 90% of fluorescent signal remained after 30 minutes, indicating good optical stability (Figure 5A). Only compound **2** showed 30% photobleaching. Although subtle, it is interesting to note that the fluorophores without sulfonates on the aromatic rings portrayed a slightly lower photostability (**3**–**5**)(~ 88% remaining fluorescence intensity) compared to the dyes with a sulfonated side chain (**6**–**11**)(95% remaining fluorescence intensity). This indicates that the substitution of sulfonates on the aromatic rings positively affects the optical stability of the fluorophores.

Earlier studies have underlined that it is also important that the dyes are chemically stable in an *in vivo* environment [8,35]. To evaluate the chemical stability of the dyes towards endogenous

nucleophiles, they were incubated for up to 6 hours at 37 °C in a model buffer containing 0.5 mM glutathione [8,36]. UPLC-MS was used to discriminate if any adducts were formed by reaction with the respective thiol. As apparent from Figure 5B, all fluorophores remained stable and fluorescent at the given conditions. This finding excludes the formation of unwanted products during *in vivo* administration, as was previously reported for the NIR dyes ZW800-1 and IRdye 800-CW [8].

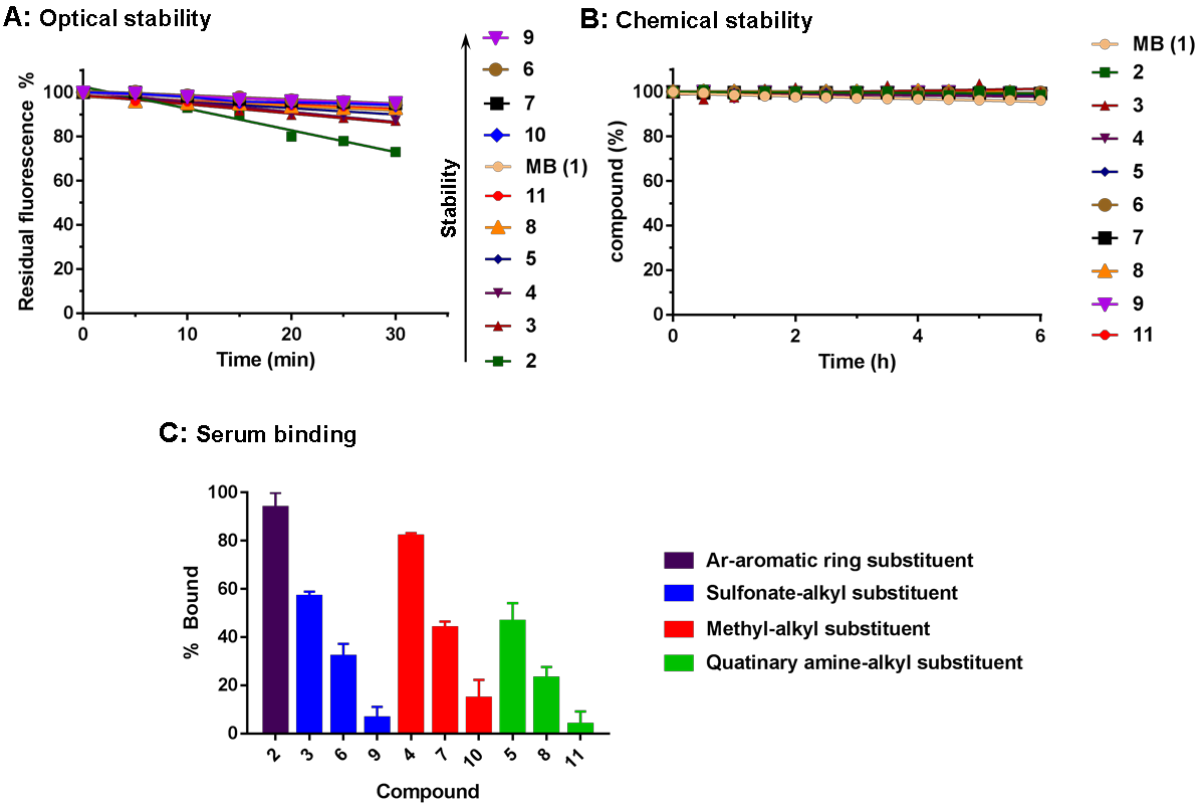

Figure 5. Optical and chemical stability of the fluorophores and their tendency to interact with serum proteins. A) Optical stability; the dyes were illuminated using the light source of a prototype Karl Storz camera setup (λ_{ex} = 590–680 nm). Reduction in fluorescence was measured up to 30 min with 5-minute intervals. In the legend the dyes are given in order of decreasing stability (arrow). B) Chemical stability of the eleven dyes in 0.5 mM glutathione in HEPES (pH 7.4) at 37 °C as assayed overtime by UPLC-MS. C) Percentage of fluorophore bound to serum proteins after 18 h of dialysis with serum versus PBS. The fluorophores are grouped in colour by their alkyl substituents and within each group the dye with non-, one-, and two sulfonates on the aromatic ring are given from left to right.

3.4 Serum protein interaction

Next to the stability of the fluorophores towards endogenous nucleophiles, the tendency of the dyes to non-covalently bind to serum proteins was also evaluated. Equilibrium dialysis against serum (18 h) revealed clear differences between the dyes (Figure 5C). Increasing the number of sulfonates on the aromatic ring induced an approximate 50% decrease in serum protein binding following each sulfonate introduced. Introducing a sulfonate on the side chain reduced the albumin interaction with about 30% compared to the neutral (Me-) substituted dyes. The quaternary-amine substituents reduced this even further. When these findings were related to the cLog P values, it appeared that there is a threshold value at cLog P = 0.8. For dyes portraying a cLog P above this value, *i.e.* lipophilic dyes, a serum protein binding tendency of > 50% was observed (compound **2**, **3** and **4**). When the cLog P value drops below 0.8, the influence of the lipophilicity seems to become less substantial and the number of charges on the compounds started to play a role, with the lowest percentage of binding found for compound **9** and **11** (< 10%, five total charges). Overall, both the aromatic substituents and alkyl substituents play a prominent role in the interaction with serum proteins.

3.5 Stacking behaviour

Previously we found that the degree of dye stacking observed in the reaction mixture was predictive for the amount of stacking of the dyes on the obtained conjugation products [8]. In general, the presence of multiple (stacked) dyes on the final product reduces the brightness and homogeneity of the sample. Therefore, the stacking-based aggregation rates of the eleven compounds investigated were determined in DMSO, PBS and H_2O at concentrations ranging from 0.3 to 100 µM. Compounds **3**–**11** did not aggregate in these solvents (Figure 6, for further details see Ref [22]), while **MB** and compound **2** did demonstrate distinct stacking in the aqueous media (Figure 6). Compound **2** showed aggregation at concentrations higher than 2.5 µM in PBS and H_2O. A comparable aggregation tendency was reported earlier for **ICG** [8]**.** Based on this, the observed stacking at > 2.5 µM concentration in aqueous medium seems to be induced by the presence of the

two additional aromatic rings. **MB** showed an even stronger dimeric stacking tendency than compound **2**, while the concentration dependency of this effect was comparable to that of compound **2** (Figure 6)[24].

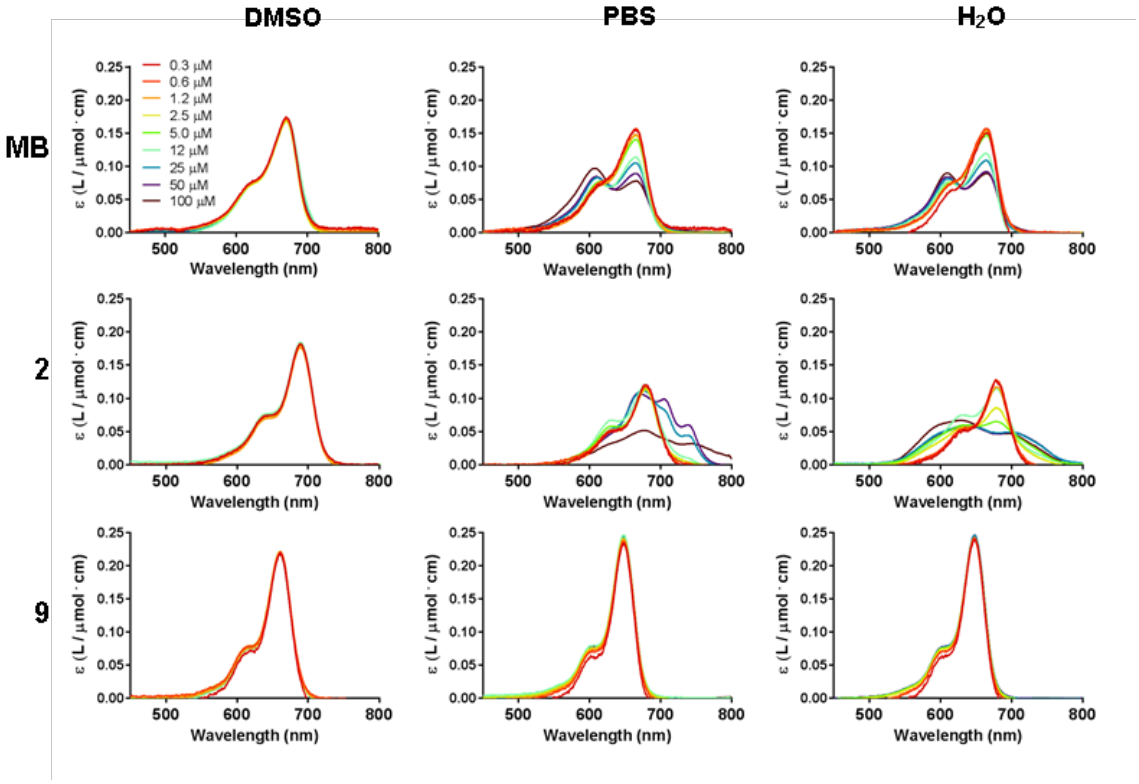

Figure 6. The stacking concentration dependency of **MB** and compound **2**, and **9** measured in DMSO, PBS and H_2O at concentrations ranging from 0.3 to 100 µM. Compound **9** is shown as model for compound **3**–**11** as they were all comparable. For detailed visualisation of each compound separately please refer to Ref [22].

3.5 Conjugation

To investigate if the structure variations in the fluorophores have an influence on their conjugation characteristics, compounds **2**–**11** were activated (yielding compound **12**–**21,** see SI) and conjugated to the reference protein Ubiquitin. This small (~ 8.5 kDa) [37], well-known regulatory protein is present in almost every eukaryotic cell and contains 7 lysine residues of which 6 are solvent-exposed (Figure 7A)(evaluated from the PDB structure 5DK8). The low molecular weight of Ubiquitin makes it possible to study the labelling process *via* mass spectrometry (MS), which helps provide insight into

the homogeneity of the products obtained within a single sample. Relating these findings to the absorbance profiles of the same products allowed for the determination of relative labelling ratios.

The labelling with the fluorophore **2** was unsuccessful due to its low solubility at the required concentrations (100 μM). Thus, the conjugation reactions yielded nine Ubiquitin constructs (**22**–**30**). While previously no stacking was observed at the concentrations used in the reaction mixture (Figure 6), absorption spectra of the conjugation products **22**, **23**, **25, 26**, and **29** revealed stacking (Figure 7B)**.** The prescence of sulfonate groups on the aromatic ring decreased the stacking as did the precence of a quatenary amine on the side chain. When measured in DMSO, these stacking interactions were no longer present due to increased solvation of the dyes (Figure S2) and the dye loading rates could be accurately determined (Figure 7B; LR)[8]. The calculated loading rates were found to be comparable (around 1) with exception of compounds **25** (1.7) and **29** (1.6). However, except for being the only two dyes with a -2 net charge (Figure 3) there is no clear indication why these loading rates were higher than the others.

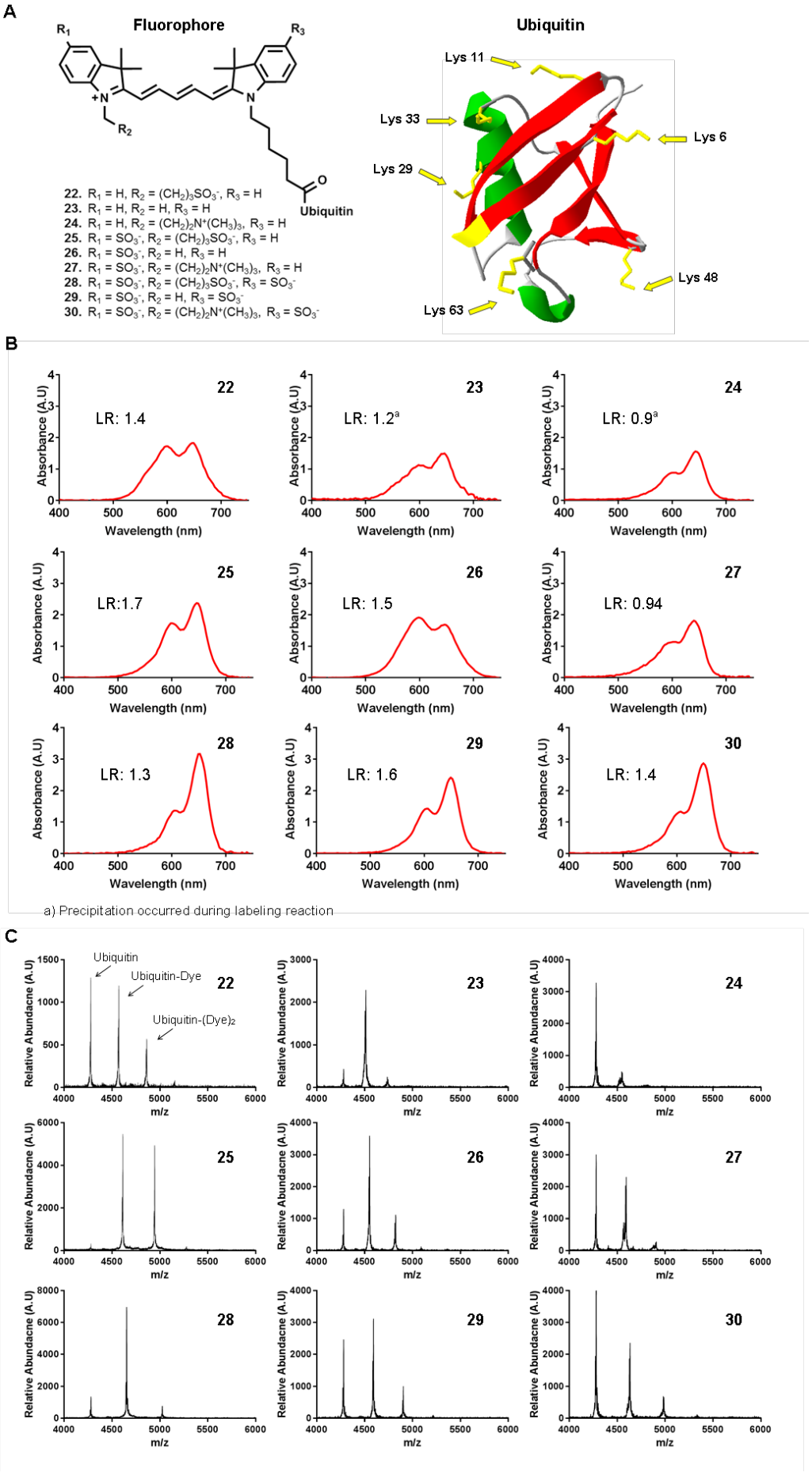
A
Fluorophore
Ubiquitin
Lys 11
Lys 33
Lys 6
Lys 29
Lys 48
Lys 63
22. R1 = H, R2 = (CH2)3SO3-, R3 = H
23. R1 = H, R2 = H, R3 = H
24. R1 = H, R2 = (CH2)2N+(CH3)3, R3 = H
25. R1 = SO3-, R2 = (CH2)3SO3-, R3 = H
26. R1 = SO3-, R2 = H, R3 = H
27. R1 = SO3-, R2 = (CH2)2N+(CH3)3, R3 = H
28. R1 = SO3-, R2 = (CH2)3SO3-, R3 = SO3-
29. R1 = SO3-, R2 = H, R3 = SO3-
30. R1 = SO3-, R2 = (CH2)2N+(CH3)3, R3 = SO3-
B
22
LR: 1.4
23
LR: 1.2a
24
LR: 0.9a
25
LR:1.7
26
LR: 1.5
27
LR: 0.94
28
LR: 1.3
29
LR: 1.6
30
LR: 1.4
Absorbance (A.U)
Wavelength (nm)
a) Precipitation occurred during labeling reaction
C
Ubiquitin
Ubiquitin-Dye
Ubiquitin-(Dye)2
Relative Abundacne (A.U)
m/z

362

Figure 7. A) The Cy5 dyes conjugated to Ubiquitin. Within the structure of Ubiquitin the surface-exposed lysine groups and the N-terminus are indicated in yellow as probable binding sides for the fluorophores. The image was constructed from the PDB structure 5DK8. B) Absorption spectra of the dyes conjugated to Ubiquitin (**22**–**30**) measured in PBS, including the dye loading rates (LR). The fluorophores on construct **22**, **23**, **25, 26**, and **29** are stacking as is indicated by the increase of the right shoulder peak. The spectra are normalised on dye concentration to underline the differences in the shape of the absorbances. C) Mass spectra of the conjugated Cy5–Ubiquitin compounds. The mass signals of M^{2+} are shown as these were the most intense, with m/z = 4278 non-conjugated Ubiquitin, m/z ≈ 4500 mono-conjugated Ubiquitin and m/z ≈ 4800 di-conjugated Ubiquitin.

When looking at the mass spectra of the conjugated Cy5-Ubiquitin compounds (**22**–**30**) it becomes evident that the samples are heterogeneously labelled and that this effect differs between dyes (Figure 7C). For the dyes with the sulfonated side chain (**22, 25, 28**), only the fluorophore with two aromatic sulfonates (**28**) labelled homogenously. For the dyes containing the methyl side chain (**23, 26, 29**) however, lower number of sulfonates on the aromatic rings resulted in a more homogenously labelled Ubiquitin (**23**). MS analysis of the compounds with a quaternary amine on the side chain (**24, 27, 30**) was more complex. The low ionisation of the mono or di-conjugated Ubiquitin resulted in a discrepancy between the information obtained by MS and what was calculated from the absorbance spectra. However, it can be concluded that also here the labelling was heterogeneous as multiple peaks were visible. Combining the absorbance and MS data, we demonstrated that while absorption spectra clearly indicate that the Cy5 dyes undergo a significant degree of stacking (in PBS Figure 7B, not in DMSO; Figure S2), the same samples only displayed a limited amount of di-conjugated Ubiquitin products (Figure 7C). Furthermore, no stacking was observed for the free form of these compounds at the same concentration (Figure 4, Figure 3 in Ref [22]). This suggests that the stacking observed is not the traditional dye–dye stacking, but comes from stacking interactions with, *e.g.* tyrosine, tryptophan, or phenylalanine amino acids within the protein. According to the crystal structure of Ubiquitin, there is at least one phenylalanine spatially

nearby every solvent-exposed Lysine (determined from the PDB structure 5DK8). The stacking interaction with the surrounding amino-acids is also be noted by the quantum yield (Table 1). After conjugation to the protein, the quantum yield of most compounds decreased, and the degree of reduction correlated with the observed amount of stacking. Indeed, also the diminishing quantum yield did not depend on whether the Ubiquitin is homogeneously labelled (one peak on the MS data), thus underlining the fact that the observed stacking occurs between the dye and neighbouring amino acids.

When the investigated dyes were compared in a biodistribution study with RGD it was found that compound **7** yielded superior *in vivo* properties [17]. Based on the chemical characteristics investigated herein however, compound **7** did not stand out, pointing out that chemical characteristics are only one aspect in the development of efficient fluorescent tracers for *in vivo* use. In the end, the Cy5 dye becomes but a component of a larger molecular structure, of which the overall characteristics drive the targeting behaviour and biodistribution [17]. Given the apparent balance that has to be obtained between the chemical characteristics of the dye and a targeting vector, it seems to be inevitable that labelling of an individual targeting vector goes hand-in-hand with screening of different Cy5-dyes structures, *e.g.* as presented in Figure 3. Nevertheless, in fluorescent tracer design we would like to suggest that only dyes are used that are: (photo-)chemically stable, bright enough to obtain a signal-to-background ratio of at least 2 with the cameras intended for clinical use, show no stacking in solution, and ideally label proteins homogeneously.

4. Conclusion

In this study, the characteristic chemical and photophysical properties of ten systematically altered Cy5 derivatives and their Ubiquitin conjugates were methodically analysed. Next to these structure–activity relationships, the compatibility of the dyes with a clinical-grade fluorescence laparoscope was also presented. Overall, the influence of the aromatic- and alkyl substituents on the chemical-

and photophysical properties of the ten Cy5 dyes has been documented more clearly, providing a solid basis for future tracer developments.

Acknowledgements

The research leading to these results has received funding from the European Research Council (ERC) under the European Union's Seventh Framework Program FP7/2007-2013 (Grant No. 2012-306890), a Netherlands Organization for Scientific Research STW-VIDI grant (Grant No. STW BGT11272). We thank KARL STORZ Endoskope GmbH & Co. KG for providing the prototype Cy5 light source. We also like to thank A.R.P.M. Valentijn for making his lab available and providing the Waters Acquity UPLC-MS system.

References

[1] Ferrari E, Gu C, Niranjan D, Restani L, Rasetti-Escargueil C, Obara I, et al. Synthetic self-assembling clostridial chimera for modulation of sensory functions. Bioconjug Chem 2013;24:1750–9. doi:10.1021/bc4003103.

[2] van Leeuwen FWB, Hardwick JCH, van Erkel AR. Luminescence-based Imaging Approaches in the Field of Interventional Molecular Imaging. Radiology 2015;276:12–29. doi:10.1148/radiol.2015132698.

[3] Byrne WL, Delille A, Kuo C, de Jong JS, van Dam GM, Francis KP, et al. Use of optical imaging to progress novel therapeutics to the clinic. J Control Release 2013;172:523–34. doi:10.1016/j.jconrel.2013.05.004.

[4] van Leeuwen FWB, Valdés-Olmos R, Buckle T, Vidal-Sicart S. Hybrid surgical guidance based on the integration of radionuclear and optical technologies. Br J Radiol 2016;89:20150797. doi:10.1259/bjr.20150797.

[5] Yuan L, Lin W, Zheng K, He L, Huang W. Far-red to near infrared analyte-responsive fluorescent probes based on organic fluorophore platforms for fluorescence imaging. Chem

442 Soc Rev 2013;42:622–61. doi:10.1039/c2cs35313j.
443 [6] Benson R., Kues HA. Fluorescence Properties of Indocyanine Green as Related to
444 Angiography. Phys Med Biol 1978;23:159–63.
445 [7] Azhdarinia A, Wilganowski N, Robinson H, Ghosh P, Kwon S, Lazard ZW, et al. Characterization
446 of chemical, radiochemical and optical properties of a dual-labeled MMP-9 targeting peptide.
447 Bioorganic Med Chem 2011;19:3769–76. doi:10.1016/j.bmc.2011.04.054.
448 [8] Van Der Wal S, Kuil J, Valentijn ARPM, Van Leeuwen FWB. Synthesis and systematic
449 evaluation of symmetric sulfonated centrally C-C bonded cyanine near-infrared dyes for
450 protein labelling. Dye Pigment 2016;132:7–19. doi:10.1016/j.dyepig.2016.03.054.
451 [9] Verbeek FPR, Vorst JR Van Der, Schaafsma BE, Swijnenburg R, Gaarenstroom KN, Elzevier HW,
452 et al. Intraoperative Near Infrared Fluorescence Guided Identification of the Ureters Using
453 Low Dose Methylene Blue : A First in Human Experience. JURO 2013;190:574–9.
454 doi:10.1016/j.juro.2013.02.3187.
455 [10] Hossam M, Askar SM. Minimally invasive , endoscopic assisted , parathyroidectomy (MIEAP)
456 with intraoperative methylene blue (MB) identification. Egypt J Ear, Nose, Throat Allied Sci
457 2012;13:25–30. doi:10.1016/j.ejenta.2012.02.003.
458 [11] Sari YS, Tunali V, Tomaoglu K, Karagöz B, İ AG, Karagöz İ. Can bile duct injuries be prevented?
459 “A new technique in laparoscopic cholecystectomy.” BMC Surg 2005;4:4–7.
460 doi:10.1186/1471-2482-5-14.
461 [12] FDA. Serius CNS reactions possible when methylene blue is given to patients taking certain
462 psychiatric medications 2011. https://www.fda.gov/Drugs/DrugSafety/ucm263190.htm.
463 [13] Mujumdar RB, Ernst L a, Mujumdar SR, Lewis CJ, Waggoner a S. Cyanine dye labeling
464 reagents: sulfoindocyanine succinimidyl esters. Bioconjug Chem 1993;4:105–11.
465 [14] Burggraaf J, Kamerling IMC, Gordon PB, Schrier L, Kam ML De, Kales AJ, et al. Technical
466 Reports Detection of colorectal polyps in humans using an intravenously administered
467 fluorescent peptide targeted against c-Met. Nat Med 2015;21. doi:10.1038/nm.3641.

[15] Phillips E, Penate-medina O, Zanzonico PB, Carvajal RD, Mohan P, Ye Y, et al. Clinical translation of an ultrasmall inorganic optical-PET imaging nanoparticle probe. Nanomedicine 2014;6:1–9.

[16] Kuil J, Buckle T, Oldenburg J, Yuan H, Borowsky AD, Josephson L, et al. Hybrid peptide dendrimers for imaging of chemokine receptor 4 (CXCR4) expression. Mol Pharm 2011;8:2444–53. doi:10.1021/mp200401p.

[17] Bunschoten A, van Willigen DM, Buckle T, van den Berg NS, Welling MM, Spa SJ, et al. Tailoring Fluorescent Dyes To Optimize a Hybrid RGD-Tracer. Bioconjug Chem 2016;27:1253–8. doi:10.1021/acs.bioconjchem.6b00093.

[18] Zhou Y, Kim Y, Milenic DE, Baidoo KE, Brechbiel MW. In Vitro and In Vivo Analysis of Indocyanine Green-Labeled Panitumumab for Optical Imaging - A Cautionary Tale. Bioconjug Chem 2014;25:1801–10. doi:10.1021/bc500312w.

[19] Bunschoten A, Buckle T, Kuil J, Luker GD, Luker KE, Nieweg OE, et al. Targeted non-covalent self-assembled nanoparticles based on human serum albumin. Biomaterials 2012;33:867–75. doi:10.1016/j.biomaterials.2011.10.005.

[20] Bunschoten A, Buckle T, Visser NL, Kuil J, Yuan H, Josephson L, et al. Multimodal Interventional Molecular Imaging of Tumor Margins and Distant Metastases by Targeting αvβ3 Integrin. ChemBioChem 2012;13:1039–45. doi:10.1002/cbic.201200034.

[21] Buckle T, Bunschoten A, Buckle T, Leeuwen AC Van, Chin PTK. A self-assembled multimodal complex for combined pre- and intraoperative imaging. Nanotechnology 2010;21:1–9. doi:10.1088/0957-4484/21/35/355101.

[22] Spa SJ, Hensbergen A, van der Wal S, Kuil J, van Leeuwen F. Data in Brief. Data Br n.d.:Submitted.

[23] Pace CN, Vajdos F, Fee L, Grimsley G, Gray T. How To Measure and Predict the Molar Absorption-Coefficient of a Protein. Protein Sci 1995;4:2411–23. doi:10.1002/pro.5560041120.

494 [24] Bergmann K, O'Konski CT. a Spectroscopic Study of Methylene Blue Monomer, Dimer, and
495 Complexes With Montmorillonite. J Phys Chem 1963;67:2169–77. doi:10.1021/j100804a048.
496 [25] Morgounova E, Shao Q, Hackel BJ, Thomas DD, Ashkenazi S. Photoacoustic lifetime contrast
497 between methylene blue monomers and self-quenched dimers as a model for dual-labeled
498 activatable probes. J Biomed Opt 2013;18:56004. doi:10.1117/1.JBO.18.5.056004.
499 [26] Tredwell CJ, Keary CM. Picosecond time resolved fluorescence lifetimes of the polymethine
500 and related dyes. Chem Phys 1979;43:307–16. doi:10.1016/0301-0104(79)85199-X.
501 [27] Fisher NI, Hamer FM. A comparison of the absorption spectra of some typical symmetrical
502 cyanine dyes. Proc Roy Soc 1936:703–23. doi:10.1098/rspa.1983.0054.
503 [28] Chin PTK, Welling MM, Meskers SCJ, Valdes Olmos R a., Tanke H, van Leeuwen FWB. Optical
504 imaging as an expansion of nuclear medicine : Cerenkov-based luminescence vs fluorescence-
505 based luminescence 2013;40:1283–91. doi:10.1007/s00259-013-2408-9.
506 [29] Buckle T, Chin PTK, van den Berg NS, Loo CE, Koops W, Gilhuijs KG a, et al. Tumor bracketing
507 and safety margin estimation using multimodal marker seeds: a proof of concept. J Biomed
508 Opt 2012;15:56021. doi:10.1117/1.3503955.
509 [30] Yeung TM, Volpi D, Tullis IDC, Nicholson G a., Buchs N, Cunningham C, et al. Identifying
510 Ureters In Situ Under Fluorescence During Laparoscopic and Open Colorectal Surgery. Ann
511 Surg 2016;263:e1–2. doi:10.1097/SLA.0000000000001513.
512 [31] Mader O, Reiner K, Egelhaaf HJ, Fischer R, Brock R. Structure Property Analysis of
513 Pentamethine Indocyanine Dyes: Identification of a New Dye for Life Science Applications.
514 Bioconjug Chem 2004;15:70–8. doi:10.1021/bc034191h.
515 [32] Levitus M, Ranjit S. Cyanine dyes in biophysical research: the photophysics of polymethine
516 fluorescent dyes in biomolecular environments. Q Rev Biophys 2011;44:123–51.
517 doi:10.1017/S0033583510000247.
518 [33] Netzel TL, Nafisi K, Zhao M, Lenhard JR, Johnson I. Base-Content Dependence of Emission
519 Enhancements, Quantum Yields, and Lifetimes for Cyanine Dyes Bound to Double-Strand

520 DNA: Photophysical Properties of Monomeric and Bichromophoric DNA Stains. J Phys Chem
521 1995;99:17936–47. doi:0022-365419512099-17936.
522 [34] Schobel U, Egelhaaf H, Frohlich D, Brecht A, Oelkrug D, Gauglitz G. Mechanisms of
523 Fluorescence Quenching in Donor – Acceptor Labeled Antibody – Antigen Conjugates. J
524 Fluoresc 2000;10:147–54. doi:10.1023/A:1009443125878.
525 [35] Cilliers C, Nessler I, Christodolu N, Thurber GM. Tracking Antibody Distribution with Near-
526 Infrared Fluorescent Dyes: Impact of Dye Structure and Degree of Labeling on Plasma
527 Clearance. Mol Pharm 2017:acs.molpharmaceut.6b01091.
528 doi:10.1021/acs.molpharmaceut.6b01091.
529 [36] Costa CM da, Santos RCC dos, Lima ES. A simple automated procedure for thiol measurement
530 in human serum samples. J Bras Patol E Med Lab 2006;42. doi:10.1590/S1676-
531 24442006000500006.
532 [37] Goldstein G, Scheid M, Hammerling U, Schlesinger DH, Niall HD, Boyse EA. Isolation of a
533 polypeptide that has lymphocyte-differentiating properties and is probably represented
534 universally in living cells. Proc Natl Acad Sci U S A 1975;72:11–5. doi:10.1073/pnas.72.1.11.
535